Properties of as-deposited and heat-treated Ni-Mn-Ga magnetic shape memory alloy processed by directed energy deposition

Jakub Toman^a, Peter Müllner^b, Markus Chmielus^{a,*}

- ^a Department of Mechanical Engineering and Materials Science, University of Pittsburgh, Pittsburgh, PA 15261, USA
- ^b Micron School of Materials Science and Engineering, Boise State University, Boise, ID 83725, USA
- * Corresponding author: Markus Chmielus

Email addresses: jakub.toman@pitt.edu (J. Toman); chmielus@pitt.edu (M. Chmielus)

Abstract

Ni-Mn-Ga magnetic shape memory alloy was processed by laser metal deposition, an additive manufacturing method. Powder used for deposition was crushed from a cast 10M martensite Ni-Mn-Ga ingot. The deposited sample was ferromagnetic and showed a 14M martensite with no detectable macroscopic composition differences throughout, except for a thin layer between substrate and deposit. Layer-by-layer deposition resulted in a layered microstructure due to differences in local thermal histories, and the sample's broad transformation temperature range is proposed to originate from the resulting variations in microstructure. Although the sample is clearly polycrystalline, columnar grains span deposition layers, which is potentially favorable to twin boundary motion. After a homogenizing and ordering heat treatment, transformations regained a typical narrow hysteresis and saturation magnetization increased, while grain growth and/or recrystallization took place. The results show the promise of laser-based additive manufacturing processes for production of magnetic shape memory alloys.

Keywords

Ferromagnetic shape memory alloy; Rapid solidification; Direct laser deposition; Additive manufacturing.

Introduction

Ni-Mn-Ga alloys have seen intense research interest as magnetic shape memory alloys (MSMAs) [1], magnetocaloric materials [2,3] and high-temperature shape memory alloys [4]. As MSMAs, single crystals of these alloys experience a reversible pseudoplastic strain of up to 10 % under application of a magnetic field [5] (12 % has been shown for Ni-Mn-Ga-Co-Cu [6]). Reversing this strain magnetically or mechanically completes a cycle, which has been practically demonstrated at frequencies of up to 1 kHz [7] and over millions of cycles [8,9]. This unique combination of properties leads to potential application as actuators [10], pumps [11], sensors [12] or energy harvesters [13].

The magnetomechanical properties of Ni-Mn-Ga depend foremost on crystal structure – and hence on composition [14] - but also on operating temperature [15]. Martensites, including nonmodulated (NM), ten-layered (10M) and fourteen-layered (14M) modulated martensite contain twins which may or may not be mobile under an applied magnetic field. Growth of a twin (or twins), with requisite twin boundary motion, is responsible for magnetic field-induced strain (MFIS) [16]. If MFIS is possible, its maximum value and the minimum magnetic field required to produce this motion are directly tied to the crystal structure [17], while the required field also depends on the difference between the operating temperature and the austenite start temperature due to change in the twinning stress [15] for type I twins [18]. For NM martensite, large MFIS has been shown only after addition of Co and Cu [6], while 14M martensite offers larger MFIS than 10M but with a higher twinning stress and thus higher required magnetic field [19]. Importantly, MFIS is only possible while the material is ferromagnetic, i.e. below its Curie temperature (T_c) . Still, even if the aforementioned requirements are satisfied, the presence of grain boundaries, e.g. in polycrystalline samples, will reduce or prevent twin boundary motion. Significant MFIS has only been reported in single crystals, in specially produced polycrystalline directional castings (1 %) [19] and in foams (up to 8.7 %) [20]. However, the processing methods for these forms are time-intensive and limit the possible shapes of MSMA elements, which are difficult to machine due to their brittleness. Recently, sintered binder jet printed Ni-Mn-Ga samples were investigated as a path to addressing these challenges [21,22].

Difficult-to-machine materials have seen a wealth of attempts to produce them by additive manufacturing methods, including directed energy deposition (DED) methods such as laser metal deposition (LMD), used here. LMD deposits material layer-by-layer and may involve rapid

solidification, high cooling rates and remelting and reheating of preceding layers, as observed in a nickel alloy [23] and modelled for stainless steel [24,25]. Under a certain range of processing conditions, LMD can result in columnar grains, as demonstrated with nickel [23,26] and titanium [27,28] alloys. Previous work in fast or rapid solidification of Ni-Mn-Ga is limited to a few investigations of laser drilling of ingots [29,30] and of melt-spinning of ribbons [31–33]. Wang et al. [33] found that faster solidification decreased the Curie temperature and decreased saturation magnetization, while increasing the magnetic field needed to move twin boundaries. They proposed that the former effects were due to structural disorder, and the latter due to residual stress, both results of rapid solidification. The authors interpreted slope changes in magnetization curves as evidence of twin boundary motion. The present study aims at establishing whether LMD can produce ferromagnetic Ni-Mn-Ga samples with room-temperature properties appropriate for MFIS.

Experimental

To create powder for deposition, an ingot with nominal composition of Ni_{51.5}Mn_{26.3}Ga_{22.2} was manually crushed, and the resulting particles were sieved to obtain a large (54 − 106 μm) and a small (≤53 μm) size range. Morphology of the large powder size was imaged with a JEOL JSM6510 scanning electron microscope (SEM), as shown in Fig. 1. Energy dispersive spectroscopy (EDS) was performed with an Oxford Instruments system in a Zeiss Sigma 500 VP SEM on mounted, polished and uncoated powder and showed the composition as Ni_{50.6}Mn_{27.2}Ga_{22.2}.

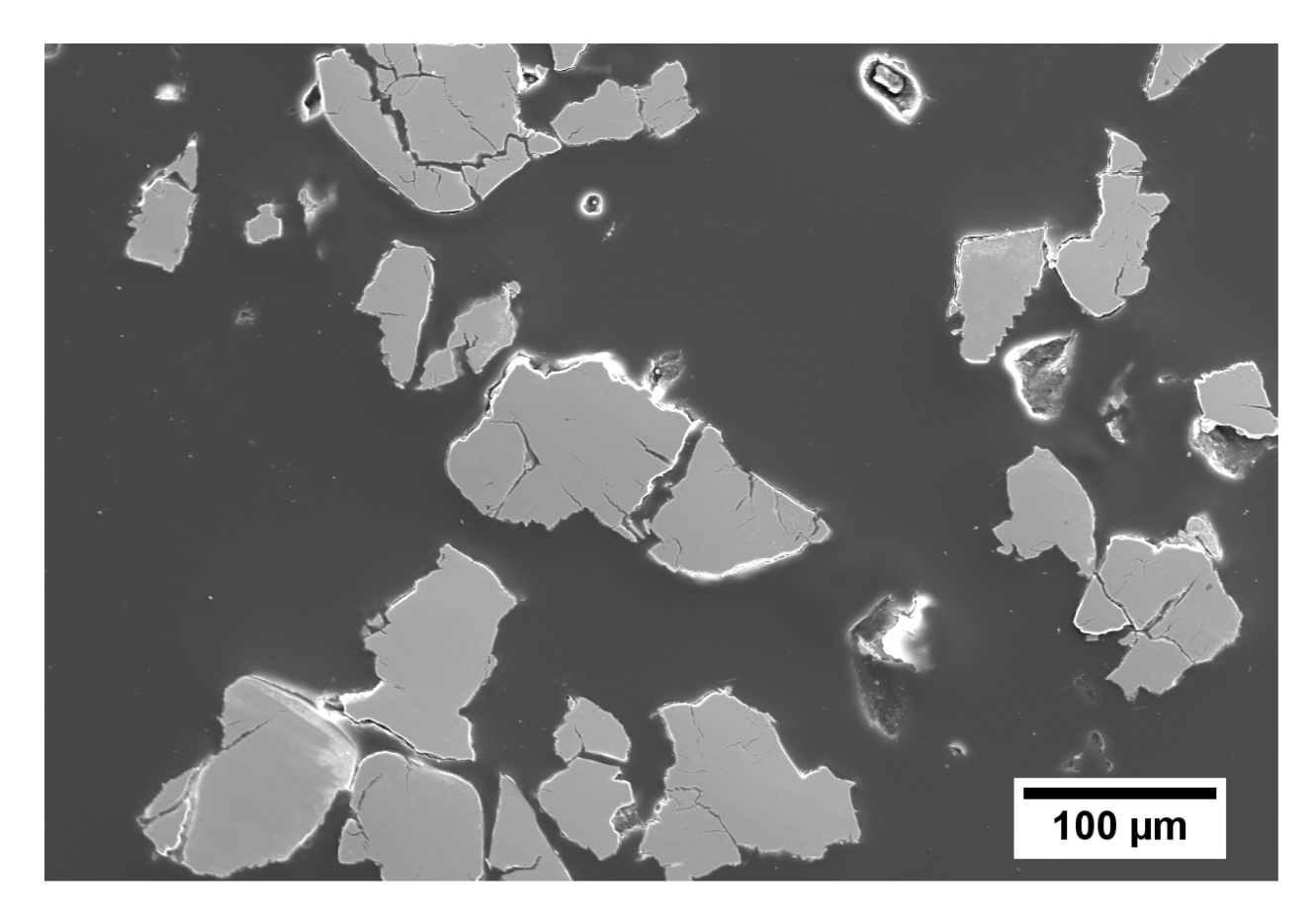


Fig. 1: Powder morphology viewed by SEM in secondary electron mode.

The large powder size was used as feedstock in a laser engineered net shaping (LENS) 450 system, which deposits material by creating a melt pool on a substrate with an Nd:YAG laser and feeding powder into this melt pool under an argon atmosphere. This method is generically known as laser metal deposition (LMD) [34], and also falls under directed energy deposition (DED). In this work, a 99.99% Ni substrate was used, an atmosphere with O₂ concentration of 0.1 ppm was achieved, and the sample was deposited at a 350 W laser power and a 2.5 mm/s travel speed. Initially, two parallel lines were deposited in opposite directions, comprising the first layer. The laser travelled 5 mm to create a line, and then was turned off for a perpendicular movement of 0.25 mm to position for the second line. For subsequent layers, the deposition head and laser spot were moved up by 0.25 mm, with laser off, and then the same pattern of lines was repeated in the same horizontal position (layers were not "rotated" relative to each other). A total of five layers was completed. The laser's path within each layer is shown schematically in Fig. 2.

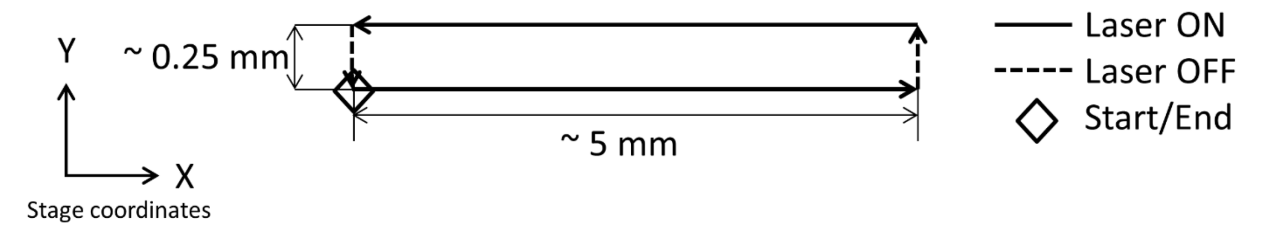


Fig. 2: Deposition path used to create samples, viewed in plane of substrate. The path was repeated identically for five layers, with each layer beginning and ending at the Start/End mark.

The as-deposited sample was sectioned and energy dispersive spectroscopy (EDS) was performed to obtain compositional information from the substrate-sample interface and from the whole of the cross-sectioned surface. For the latter, area scan results were averaged in order to determine the overall composition of the surface. Following removal of the substrate, magnetization measurements were performed in a LakeShore model 7407 vibrating sample magnetometer (VSM) as a function of field up to 1.5 T with a hysteresis loop, and as a function of temperature from 25 to 120 °C at a constant field of 50 mT after addition of a model 74034 oven. Differential scanning calorimetry (DSC) was conducted with a PerkinElmer Pyris 6 with sub-room temperature capability at a rate of 5 °C/min. The same DSC was also used for small-size powder after annealing in a sealed argon atmosphere at 800 °C for 10 h. X-ray diffraction (XRD) patterns were collected with a Bruker D8 Discover diffractometer with Cu K_α radiation. The as-deposited sample was mounted, polished and etched with a mixture of 4 mg CuSO₄ + 20 ml HCl (36.5 – 38 w/w %) + 20 ml H₂O, and imaged with a Keyence VHX-600 optical microscope. The sample was then re-polished, and heated and cooled to produce a full transformation to austenite and back to martensite while constrained by epoxy mounting. Differential interference contrast (DIC) with optical staining was used to observe the surface topography. Finally, following re-polishing, removal from mounting and encapsulation in an argon atmosphere, the sample was homogenized at 1000 °C for 24 h, ordered at 700 °C for 12 h, and furnace cooled. After this heat treatment, all characterization steps were repeated.

Results and Discussion

Effect of Deposition Process on Microstructure

Showing an overview of the etched cross-section of the sample, Fig. 3a reveals not just the overall shape of the sample, but also boundaries between portions of the deposition path¹. Fig. 3b is a magnified view of the top-left of the cross-section, and the inset c clearly shows dendritic structures within the outermost regions of the sample, with interdendritic spaces visible as dark features. The remainder of the sample, as seen in the bottom-right areas of Fig. 3b, contained similar, dark features that are largely straight but did not have the full, complex shape of interdendritic spaces. Additionally, the bottom-right of the as-deposited sample, shown in Fig. 3d, included elongated shapes which alternate in their angle relative to the horizontal. These are grains which grew approximately normal to the substrate within each layer and continued to do so across multiple deposition layers.

Overall, Fig. 3a shows that the as-deposited sample consisted of multiple, dissimilar regions. These different regions are results of: (1) the discontinuous nature of layer-by-layer deposition, and (2) the specific location within a deposited layer as it related to the outside of the deposited volume. A consequence of the first point is that the last (top) layer had a simpler thermal history in contrast to the first (bottom) layer: as a later layer was added, the preceding layer was partially remelted, and all of the previous layers were reheated to some degree, as has been

¹ Even though only 5 layers were deposited, Fig. 3a and the schematic in Fig. 5 show 9 "apparent" layers. This excess of apparent layers was caused by a small spacing between the two parallel deposition lines within the same layer (Error! Reference source not found.). This spacing was smaller than the width of deposited material of each line, causing the material within a single layer to overlap vertically. Viewed from the side, the deposited material no longer sat in the same horizontal plane. Thus, the material corresponding to parallel laser lines appears as separate layers ("apparent layers"). Each of the apparent layers is only partially visible in the specific plane of the cross-section, and so the apparent layers do not necessarily span the entire length of the sample. While ten "apparent layers" are expected, only nine are visible, most likely due to the position of the cross-section plane within the sample such that a would-be apparent layer was excluded completely.

discussed in previous studies of LMD [23–25]. Additionally, for layers which are covered by subsequent layers, volumes near the edge (near the sides of the sample) might have experienced faster cooling or lower magnitudes of reheating due to their proximity to convective cooling and their location on the outside of the two parallel laser tracks.

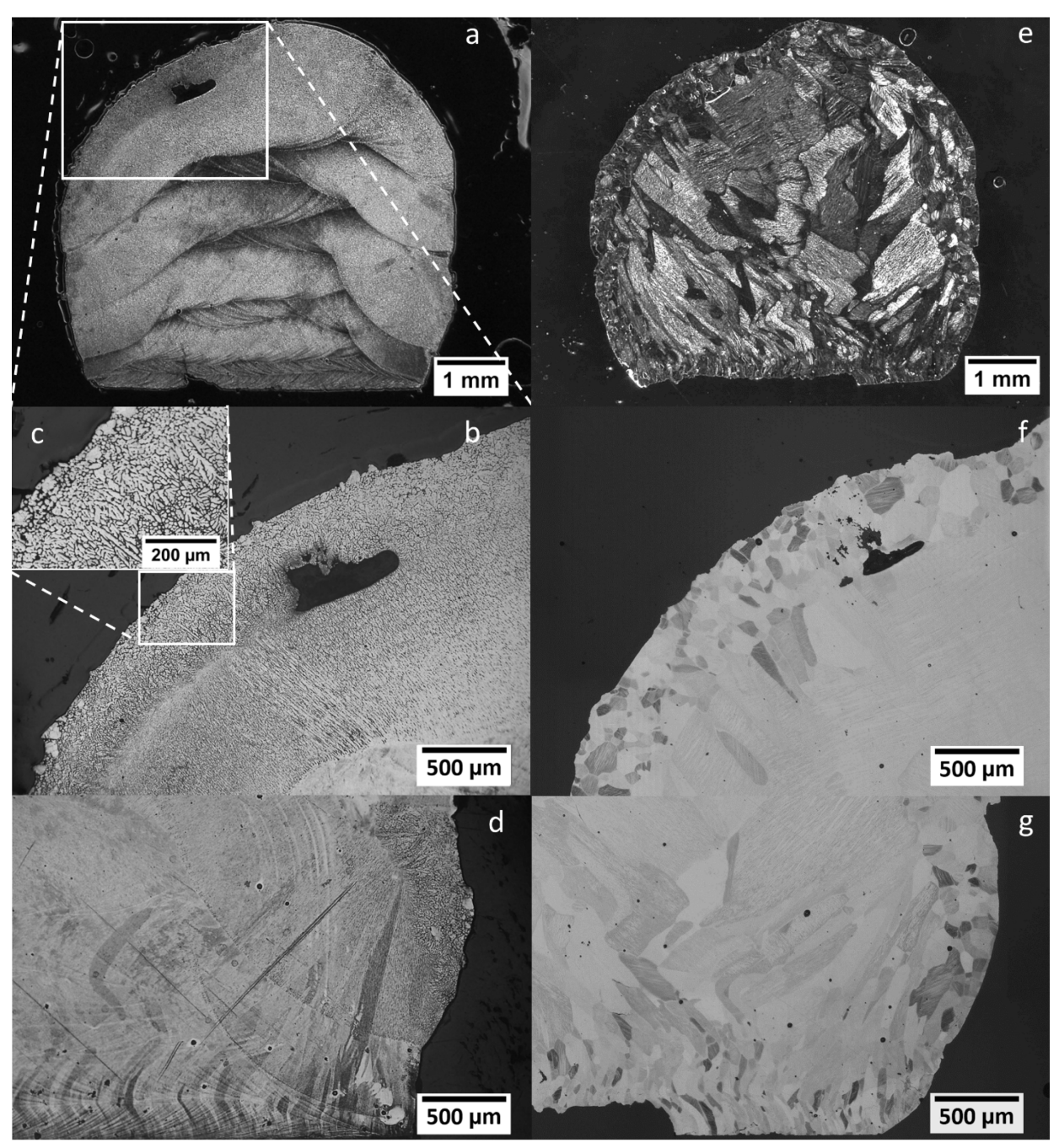


Fig. 3: Cross-sectional optical micrographs of the as-deposited (a–d) and homogenized sample (e–g) after etching. The horizontal edge visible at the bottom of (a) is the surface of the interface between the deposited samples and the substrate.

Together, these two effects created volumes within the sample that had significantly different thermal processing conditions, including (a) as-deposited regions which experienced high rates of solidification, little or no heat treatment and retained a dendritic structure, and (b) regions which have been modified by remelting and repetitive reheating to high temperatures followed by fast cooling. The latter regions contain portions of interdendritic spaces of various lengths without the remainder of the full interdendritic shapes, which were reduced by homogenization as a result of reheating. These lower, homogenized regions might be expected to be discretely different, as each preceding layer experienced one more reheating cycle than the one before it; however, this was balanced by reduced impact of later reheating cycles – in a given layer, each subsequent reheating cycle likely reached a lower temperature due to an increase in the distance from the heat source. Thus, layers near the bottom of the sample may be more similar than those near the top. Fig. 3a shows this qualitatively – the bottom-most layers are similar. These layers also have a smaller height – a result of remelting of each layer by the subsequent layer, and of wandering of one or more deposition parameters (causing a changing difference in the software layer height vs. the physical layer height). Furthermore, some areas near the top and near the edges of the sample contain dendrites (Fig. 3c). The direction of dendritic growth is heavily influenced by the temperature gradient, and generally approaches normal to the solidification front. The areas on the right of the top layer (Fig. 4) show partial remains of interdendritic spaces which do not correspond to full dendrites, and still another area further right shows only "dots" of interdendritic material. Finally, the appearance of these structures is influenced by the direction of growth relative to the sectioning plane.

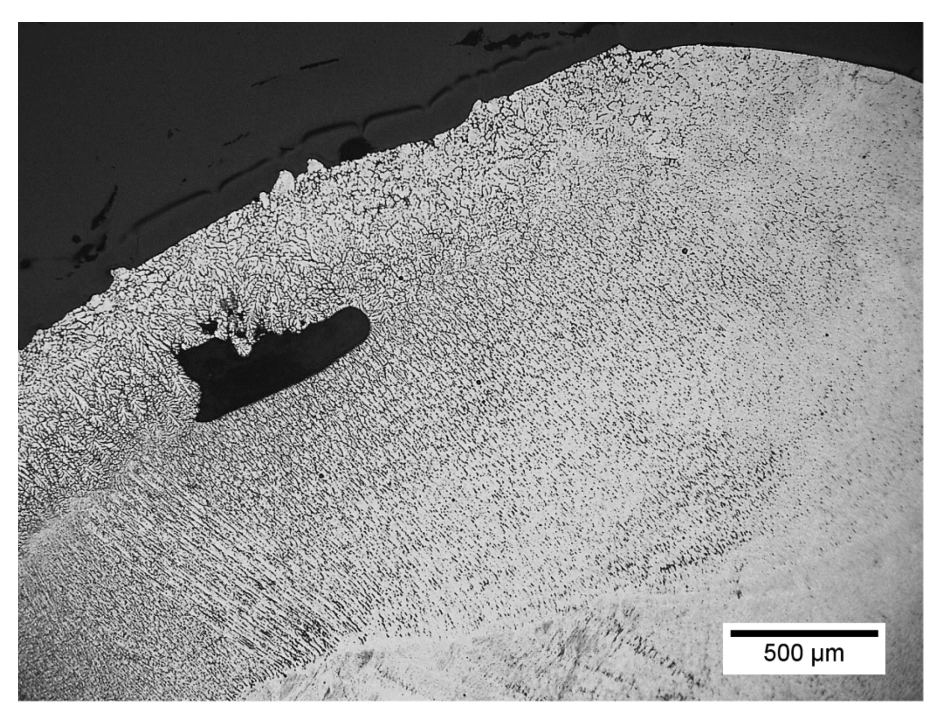


Fig. 4: Optical micrograph of the as-deposited sample after etching, showing fully dendritic, partially dendritic, and "dot"-shaped dendrite remains as one moves from left to right along the top edge of the sample.

The microstructure is summarized schematically in Fig. 5, where dendritic or partially dendritic regions are highlighted in yellow and orange and the remaining regions, with linear segments of interdendritic spaces, are shown in grey. The fact that the top of the sample shows full dendrites on the left side only may be tied to extended time at temperature for the right side, perhaps due to a single reheating cycle at temperatures near the solidus. This was caused by the right side being at the "turn-around" end of the deposition path within the top layer, resulting in a longer time at a higher temperature for that region of the layer.

The relationship between the growth direction of columnar grains within a given layer and the direction of laser travel within that layer is demonstrated in Fig. 5 (green shapes taken from grains visible in Fig. 3d).

In summary so far, microstructural characterization reveals different microstructures at different locations, reflecting the dissimilar thermal histories originating from repeated local melting and solidification.

Finally, the homogenization and ordering treatment was successful in dissolving dendrites and composition differences at deposition layer boundaries (Fig. 3(e-g)). While grains in the

lowest deposition layers appear in their original locations, the central upper regions of the sample have been considerably altered by grain growth and/or recrystallization. Central regions contain elongated grains which grew from lower layers or were already present, but the upper region contains a grain with size on the order of 1 mm, much larger than its surrounding grains. Notably, the regions near the surface previously described as "fully dendritic" have given way to equiaxed grains with size around $100 \ \mu m$ (Fig. 3f), most likely due to recrystallization.

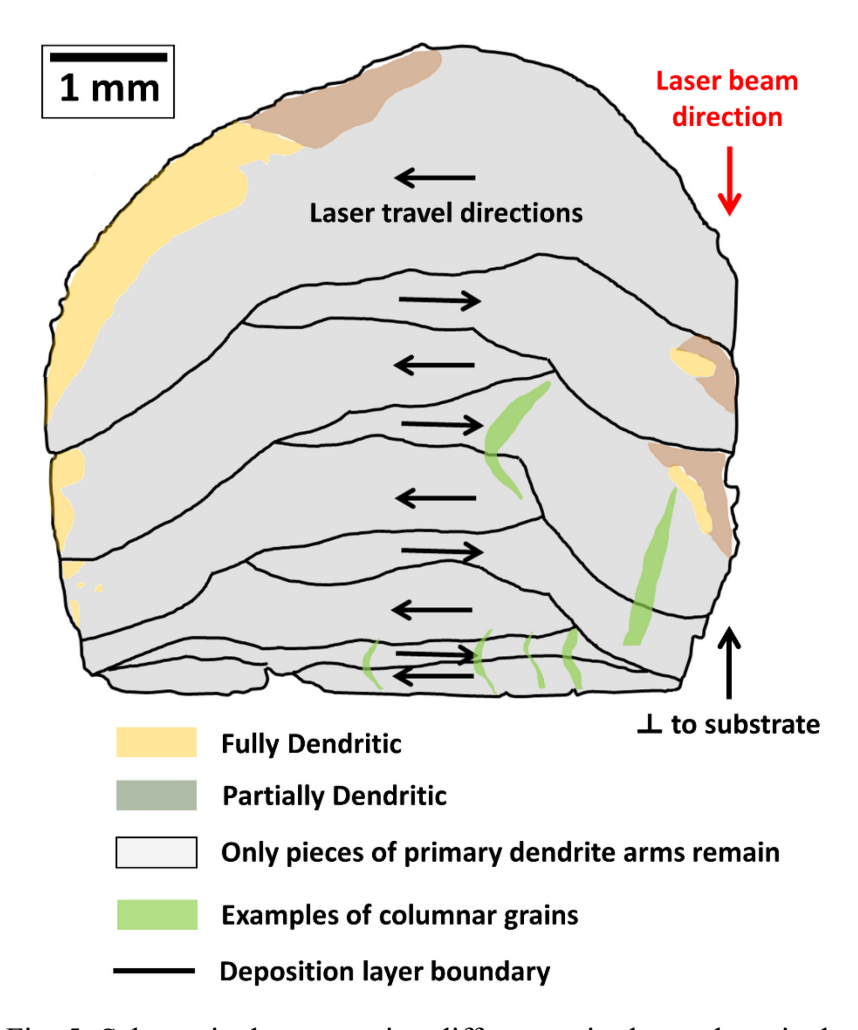


Fig. 5: Schematic demonstrating differences in the as-deposited microstructure due to regions of dissimilar thermal history.

Composition

The cross-section's overall composition, measured by EDS analysis, is given in Table 1 along with the powder's composition. The slight measured increase in Mn from powder to asdeposited sample is likely not real, but rather is caused by uncertainty, considering the large

standard deviation of the values for the powder. EDS line scans performed throughout the cross section of the sample did not show any compositional heterogeneity or changes beyond noise and uncertainty of the measurement itself.

Table 1: Composition of feedstock powder and sample in as-deposited and homogenized-and-ordered conditions obtained from EDS area spectra.

Composition [at%]						
	Ni	Mn	Ga			
Powder	50.6 ± 0.75	27.2 ± 1.81	22.2 ± 1.17			
As-deposited	50.9 ± 0.31	27.5 ± 0.28	21.6 ± 0.43			
Homogenized	51.0 ± 0.25	26.9 ± 0.23	22.1 ± 0.08			

A series of point spectra arranged in a line crossing the sample-substrate interface showed that the change from the sample's overall composition to the Ni substrate spans a distance of less than $10 \mu m$. From the thin zone of intermediate compositions found at the sample-substrate interface, we infer that little melting of the substrate took place and that the effect of the substrate on the sample's composition is limited to the very bottom of the first layer.

Homogenization and ordering resulted in a measured decrease in Mn (0.7 at.-%), likely due to evaporation.

Transformation Behavior and Relationship to Microstructure

Fig. 6 plots heat flow vs. temperature from the DSC scans for powder in the as-received condition, powder after annealing, and the as-deposited and homogenized-and-ordered conditions of the sample from 0 to 120 °C. The most important information is summarized in Table 2. For the as-received powder, no indication of transformation appeared; after annealing, the martensite transformation (upon cooling) and reverse transformation (upon heating), as well as the Curie temperature, are clearly visible, and the corresponding transformation temperatures are summarized in Table 2. The DSC curves of the as-deposited sample show a broad reverse transformation peak from 27 (A_s) to 92 °C (A_f) with three distinct slope changes and the peak at

61 °C (A_p). Upon cooling, the broad transformation to martensite took place from 87 (M_s) to 17 °C (M_f), again with three distinct slope changes and a maximum at 52 °C (M_p). After homogenization and ordering, the transformation width was reduced. From the DSC result, the widths are 11 °C for both transformations, narrower than for the as-deposited sample (65–70 °C) and even narrower than for the annealed powder (13–17 °C). Although it is difficult to locate an "average" transformation temperature for the as-deposited sample, transformations clearly shifted to higher temperatures after homogenization, perhaps by about 10 °C. This shift may correspond to slight compositional change during heat treatment (the Mn/Ga ratio changed by only 0.01, likely a smaller change than the relative error of EDS analysis) and also to relaxation of residual stresses. Results from Wang et al. [33] do not show a clear correlation between transformation temperature and degree of disorder. Additionally, the T_c values measured by DSC for the homogenized sample are lower than for the annealed powder. This may be due to either slight compositional change as mentioned, or due to incomplete homogenization and ordering: Wang et al. [33] suggested that a greater degree of disorder lowers T_c .

The magnetization for the as-deposited and homogenized-and-ordered conditions of the sample as a function of temperature (from 35 to 110 °C) are also displayed in Fig. 6. The magnetization of the as-deposited sample increased nearly linearly from the outset of heating at 35 °C until about 75 °C, where it reached its maximum. The Curie temperature T_c was 87 °C. Upon cooling, the magnetization increased below T_c until maximum magnetization and then decreased linearly again, but with a lower slope than upon heating. The higher magnetization of this phase upon cooling than upon heating was caused by the applied magnetic field which preferentially selects martensite variants with the axis of easy magnetization more closely aligned with the applied field. After homogenization and ordering, as already seen with DSC, the transformation's breadth is reduced. A 4 °C increase in T_c might suggest compositional change, as noted earlier, but the more ordered structure that is expected after the treatment should lead to an increase [31,33].

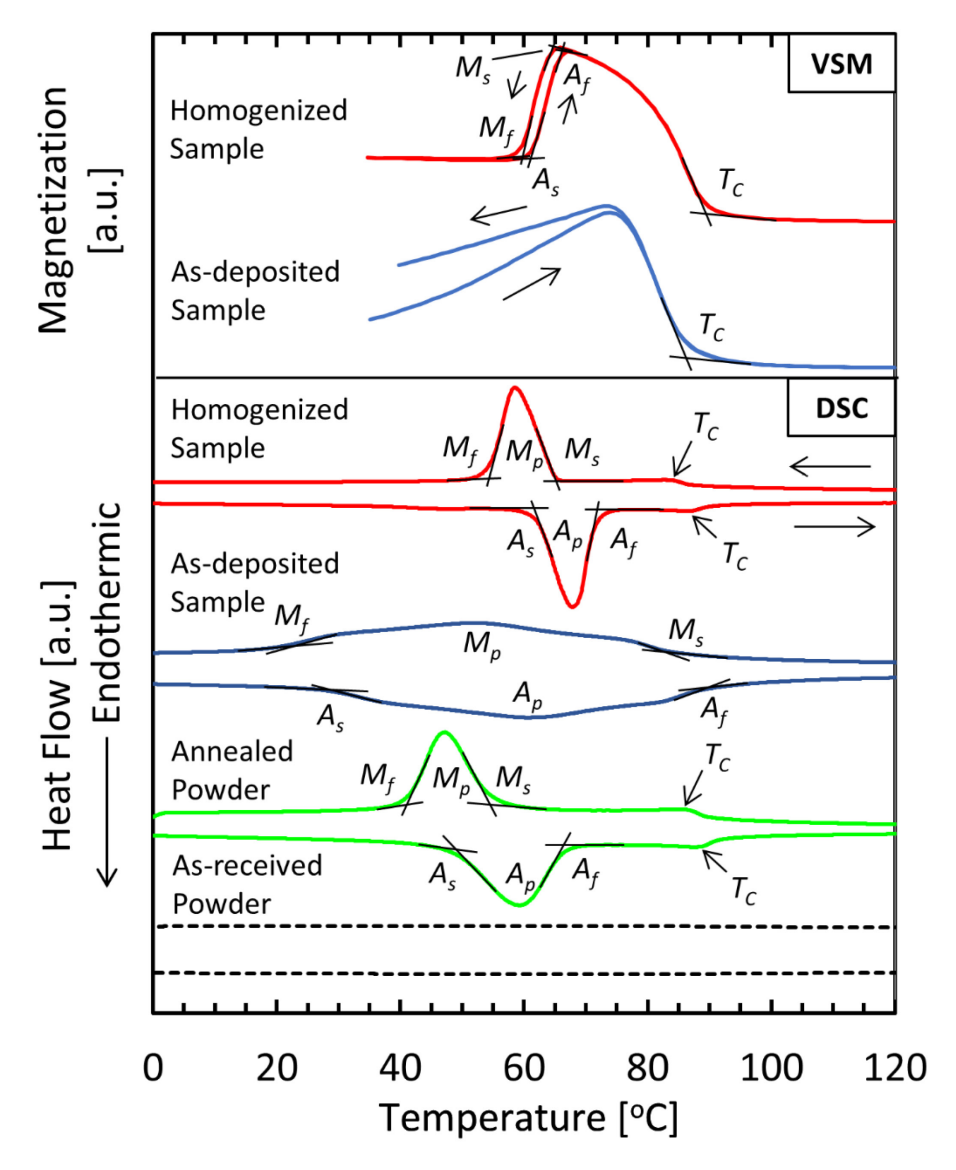


Fig. 6. DSC and magnetization vs. temperature (VSM) results for the as-received and annealed powders, as-deposited sample and homogenized-and-ordered sample. Amplitudes are not to scale.

Table 2: Transformation temperatures and Curie temperatures.

	Transformation temperature [°C]						T _c [°C]	
Sample	A_s	A_{peak}	A_{f}	$M_{\rm s}$	M_{peak}	M_{f}	heating cooling	
Annealed Powder	49	59	66	54	47	41	89 86	
As-deposited Sample	27	61	92	87	52	17	86 ^a	
Homogenized Sample	62	68	73	65	59	54	87 83	
	61 ^a		66 ^a	65 ^a		59 a	90 ^a	

^a Values obtained from magnetization vs. temperature experiments. All other values obtained by DSC.

Combining the results of DSC and VSM temperature-dependent measurement creates a better understanding of the phase transformation in powder and the as-deposited sample. While the as-received powder had a suppressed phase transformation due to the high residual stresses, the annealed (stress-relieved) powder showed normal transformation behavior of a Ni-Mn-Ga MSMA. The LMD sample had an abnormal, wide transformation range of 25 – 92 °C as indicated by DSC (due to the onset of the Curie demagnetization, the complete phase transformation was not observable above 86 °C in the VSM measurement). This broad transformation behavior far exceeded those seen in heat treated single crystals [35], polycrystalline ingots [14] and powder [36]. Broad transformations should be expected given the lack of heat treatment, similarly to the up to 50 °C transformation breadth of as-cast, untreated material in [30]. Additionally, the presence of multiple, dissimilar microstructural regions discovered by etching explain the shape of the DSC result. Three additional, distinct changes in slope occurred between the start and end of each overall transformation peak, and these do not correspond to the start, peak or finish of the overall transformation. They may correspond to the regions of similar thermal history which were proposed earlier. The shift in transformation temperatures between regions may be caused by multiple factors, including compositional heterogeneity, lattice strains, and the presence of multiple martensite structures or phases. While EDS line scans did not show any conclusive

evidence of compositional heterogeneity, the differences in composition needed to produce the shifts from the main transformation peaks to the slope changes just mentioned may be on the order of 0.1 to 1 at.-% – Pötschke et al. [37] noted that shifts of 5 °C can correspond to differences of <0.1 at.-%, while Rolfs et al. [38] reported shifts on the order of 1 °C for compositional differences of about 0.5 at.-%. Therefore, compositional heterogeneity cannot be ruled out as a cause, because such small changes could not have been reliably detected by EDS. Indeed, the visibility of dendrites after etching is evidence of chemical segregation. An inhomogeneous residual stress distribution, which is common in LMD samples [39], is another likely contribution, as residual stress has been linked to shifts in the martensitic transformation temperature in Ni-Mn-Ga thin films [40,41].

Magnetic properties

Fig. 7 presents magnetization of the as-received powder, as-deposited sample and homogenized-and-ordered sample as a function of field strength (hysteresis loops). Table 3 lists ferromagnetic properties obtained from these plots and shows an increase in the magnetization of the as-deposited sample over the powder. The inset to Fig. 7 gives a detailed view of the hysteresis of the deposited sample at lower field strengths, where a notable anomaly appeared in the slope of the curve. Upon magnetic field increase, the slope of the magnetization changed abruptly. This change was not part of the rounded decrease in slope due to saturation, and did not re-appear upon field decrease. The slope change was again visible at a similar but negative field strength. Such slope changes, which reverse upon reversal of field, have been claimed to be evidence of twin boundary motion [33], although twin boundary motion has also been attributed to steps which reverse upon decreasing field directly in the first quadrant [42] or not at all [31]. Differences between the reported behaviors may be explained by dominance of either magnetoelasticity or magnetoplasticity in a given situation [43]. Therefore, it is possible that twin boundaries within some grains of the sample move over short distances.

After homogenization and ordering, the saturation magnetization of the sample increased by 10 % (Table 3). Lázpita et al. [44] showed that Mn atoms on Ga sites, which are not "proper" stoichiometric Mn sites, couple antiferromagnetically, and Wang et al. [33] reported that less-rapidly quenched Ni-Mn-Ga ribbons (smaller degree of disorder) reach higher magnetization. As annealing at 700 °C promotes order, the present increase in magnetization shows agreement with the cited articles. However, the magnetization of the homogenized sample was 14 % lower

than for a very similar composition of a homogenized single crystal [45], perhaps due to incomplete ordering. The coercive field and remanence of the sample were notably reduced, leading to softer ferromagnetic behavior and suggesting a decrease in the number of magnetic domain pinning sites such as defects and grain boundaries [46]. Furthermore, the slope changes in the hysteresis loop noted for the as-deposited sample were absent for the homogenized sample (Supplementary Figure 2), which was magnetized prior to data collection. The new behavior is more akin to that of single crystals and indicates a low density of twin boundary pinning sites. Change in twinning stress due to the shift in transformation temperatures, relative to experiment temperature, may play an additional role.

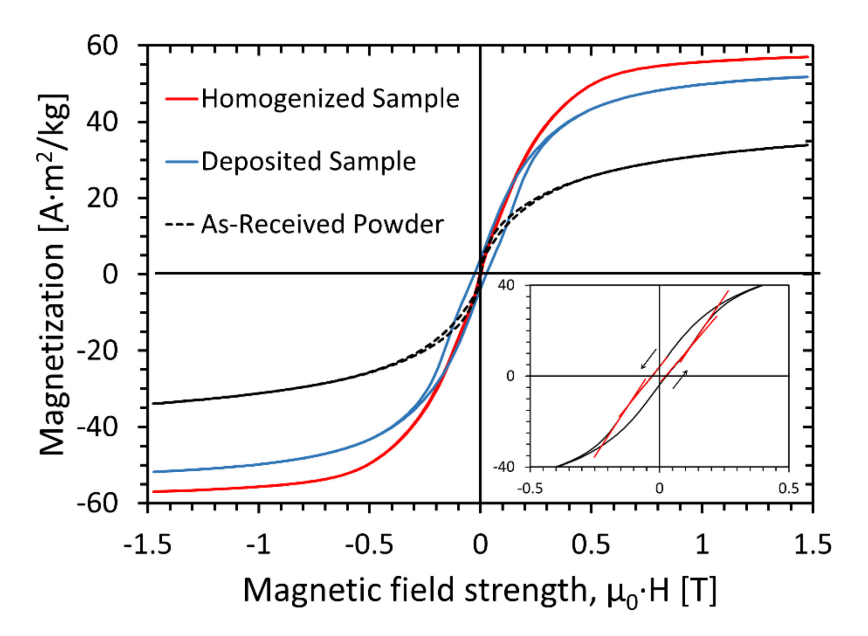


Fig. 7: Magnetization hysteresis loops for the as-received powder, as-deposited sample and homogenized sample. Inset shows view of magnetization hysteresis loop for the as-deposited sample near the origin, with tangents drawn to highlight slope changes (see Supplementary Figure 1 for larger size). Initial segments from 0 to $+H_{max}$ not shown.

Table 3: Magnetic properties: saturation magnetization M_s at 1.5 T, remanent magnetization M_r upon first decrease from maximum positive field, and coercive field H_c in the same segment.

Sample	M_s [A·m²/kg]	M_r [A·m²/kg]	<i>H_c</i> [T]
As-received Powder	33.9	0.84	-0.003
As-deposited Sample	51.8	4.07	-0.028
Homogenized Sample	57.0	0.97	-0.004

Crystal structure

While the results presented so far make it clear that the as-deposited sample was largely (although perhaps not completely) martensitic at room temperature, DIC optical microscopy and XRD were performed to confirm these findings directly. The mounted as-deposited sample was heated above A_f and allowed to cool to room temperature. A DIC micrograph, Fig. 8a, shows parallel, contrasting areas which thus possess surface gradients with opposite signs – typical of twin domains. The same was done with the homogenized sample, producing Fig. 8b, where twin variants or domains manifest themselves more clearly. The visual observation of twins after cooling through the martensite transformation further shows that martensite was present at room temperature.

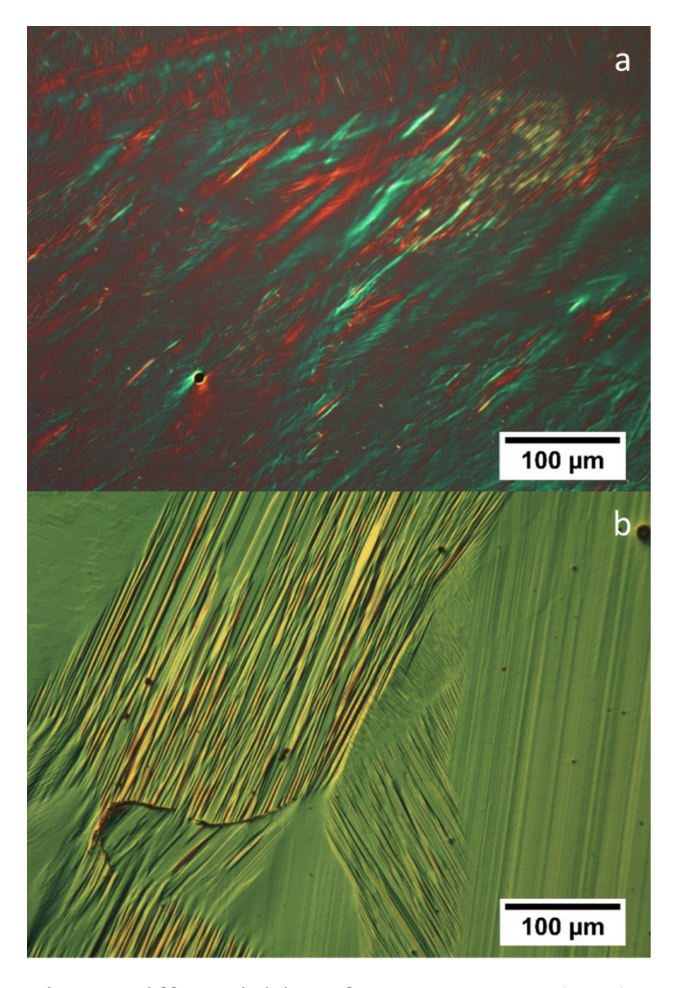


Fig. 8. Differential interference contrast (DIC) optical micrograph of the deposited sample after mounting, polishing, heating above A_f, and cooling to room temperature.

Fig. 9 displays diffractograms obtained from two orientations of the sample (rotations about the surface normal φ). The majority of identified diffraction peaks originate from the 14M martensite structure, and reflections of the 10M martensite phase were not present. By comparison to [33,35,47,48] and by indexing against calculated peak positions for the monoclinic approximations of martensite structures, the diffraction patterns overwhelmingly show the pseudo-orthorhombic structure that is associated with 14M martensite. However, some additional peaks which could not be identified are present, and may originate from modulations or other phases, but did not appear as complete sets. In the as-deposited sample, regions with some remelting and reheating dominate the cross-sectional area, and it is plausible that these regions could have incompletely transformed further transformed to the 14M structure from another due

to this thermal treatment. Insufficient counting statistics would explain the absence of further peaks and the low intensity of those present.

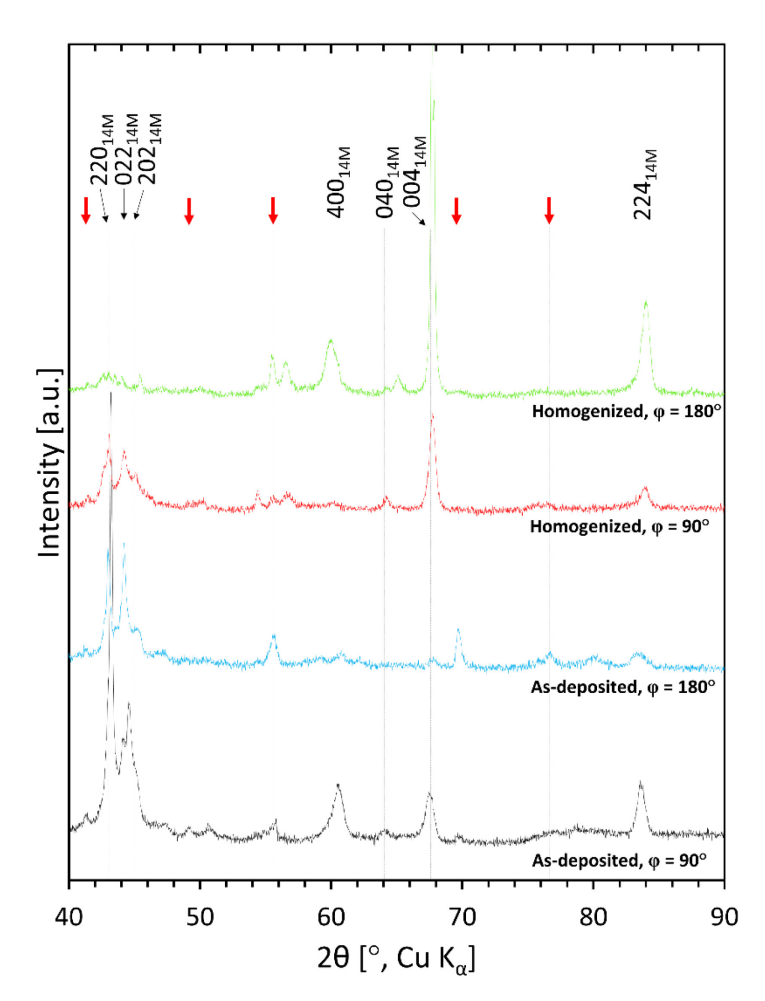


Fig. 9: Diffractograms obtained from the sample in as-deposited and homogenized-and-ordered conditions. φ is the angle of rotation about the surface normal. Red arrows indicate modulation peaks.

After homogenization and ordering, the 004 peak has overtaken the 220-type peaks as the most prominent. Since care was taken to expose the same areas of the sample to the beam, this suggests that grain growth took place during the homogenization step and positioned a larger proportion of grains with (004) planes parallel with the surface in those areas. It has been reported that heat treatment of hot extrusion samples at 1000 °C led to "maximum grain size" after just 60 minutes [49], which implies that grain growth takes place during the homogenization treatment.

Potential for twin boundary motion

The presence of 14M martensite, if viewed alone, would be promising for functionality: in Ni-Mn-Ga, 14M is capable of very large magnetic field-induced strain [5]. Additionally, the DSC and magnetization versus temperature experiments (Fig. 6) revealed that transformation occurs near room temperature, which may allow a low twinning stress. However, the presence of grain boundaries as barriers to twin boundary motion would hinder functionality. The sample also contains cracks in some regions and large voids, both of which may affect twin boundary motion. On the other hand, there is evidence of grain growth in a direction normal to the substrate in lower areas of the sample, resulting in columnar grains. Columnar grains have been reported to allow MFIS along their long axes by Gaitzsch et al. [50]. Furthermore, these grains appear to cross boundaries between deposition layers. Although grain growth after heat treatment might detract from a desirable columnar grain structure, decreasing the homogenization temperature may allow for a balance between achieving homogenization and avoiding grain growth. While it is not known whether the present sample would show any MFIS if tested magnetomechanically, under refined deposition parameters and post-deposition processing, directed energy deposition might be used to produce MSMAs with macroscopic MFIS.

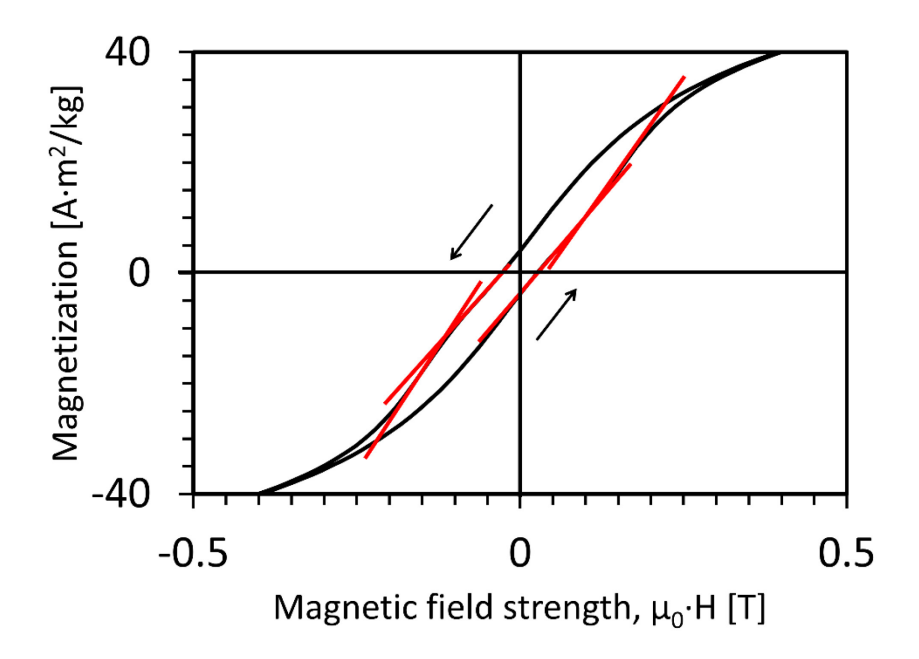
Conclusion

Ni-Mn-Ga, the most commonly studied MSMA, has been processed by laser metal deposition, a directed energy deposition additive manufacturing method. The laser-deposited material is ferromagnetic and has a majority 14M martensitic structure at room temperature. Remelting and reheating of previous layers created regions of dissimilar thermal histories, visible after etching. These microstructural differences are likely the cause of the additional slope changes in the broad martensitic transformations that were observed by DSC and of the nearly linear increase in magnetization with temperature of the as-deposited sample. Notably, magnetization of the as-deposited sample changes slope in a manner which has been associated with twin boundary motion by some authors. Homogenization and ordering dissolved dendrites, restored typical transformation breadth, increased saturation magnetization, reduced the degree of ferromagnetic hysteresis, but also caused grain growth and/or recrystallization. Based on these findings, directed energy deposition additive manufacturing methods followed by optimized post-processing may have the potential to allow cost-effective production of functional polycrystalline MSMAs with columnar grain structures and novel, otherwise difficult-to-achieve shapes.

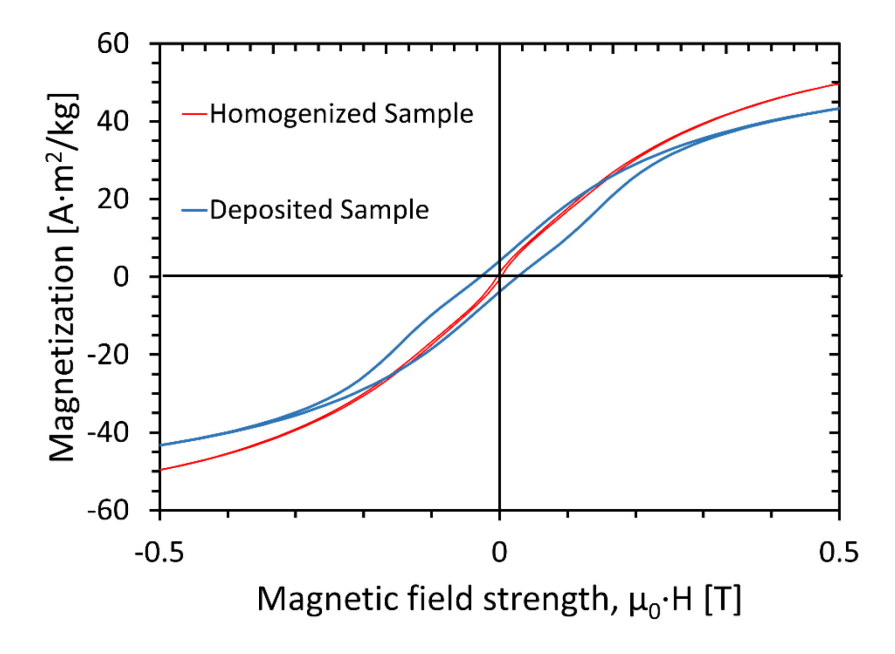
Acknowledgements

The authors thank A. Mostafaei for his comments during the preparation of this manuscript and E.L. Stevens for EDS analysis, and acknowledge partial support from the University of Pittsburgh Central Research Development Fund. J.T. is thankful to the Department of Mechanical Engineering and Materials Science and to the Frank V. Naugle Scholarship fund for financial support. This work was partially supported by the National Science Foundation grant 1727676. This work was performed in part at the Nanoscale Fabrication and Characterization Facility, a user facility of the Gertrude E. and John M. Petersen Institute of NanoScience and Engineering, and at the Materials Micro-Characterization Laboratory, both of the University of Pittsburgh.

Supplementary Figures



Supplementary Figure 1: Portion of the magnetization hysteresis loop for the as-deposited sample, with tangents drawn to highlight slope changes (presented previously as the inset of Fig. 7).



Supplementary Figure 2: Comparison of the magnetization hysteresis loops of the sample in asdeposited and homogenized-and-ordered conditions over the range of notable slope changes.

References

- [1] E. Faran, D. Shilo, Ferromagnetic Shape Memory Alloys-Challenges, Applications, and Experimental Characterization, Exp. Tech. (2015). doi:10.1111/ext.12153.
- [2] F. Hu, B. Shen, J. Sun, G. Wu, Large magnetic entropy change in a Heusler alloy Ni52.6Mn23.1Ga24.3 single crystal, Phys. Rev. B. 64 (2001) 132412. doi:10.1103/PhysRevB.64.132412.
- [3] B. Ingale, R. Gopalan, M.M. Raja, V. Chandrasekaran, S. Ram, Magnetostructural transformation, microstructure, and magnetocaloric effect in Ni-Mn-Ga Heusler alloys, J. Appl. Phys. 102 (2007). doi:10.1063/1.2751489.
- [4] J. Ma, I. Karaman, R. Noebe, High temperature shape memory alloys, Int. Mater. Rev. 55 (2010) 257–315. doi:10.1179/095066010X12646898728363.
- [5] P. Müllner, V.A. Chernenko, G. Kostorz, Large cyclic magnetic-field-induced deformation in orthorhombic (14M) Ni–Mn–Ga martensite, J. Appl. Phys. 95 (2004) 1531. doi:10.1063/1.1639144.
- [6] A. Sozinov, N. Lanska, A. Soroka, W. Zou, 12% magnetic field-induced strain in Ni-Mn-Ga-based non-modulated martensite, Appl. Phys. Lett. 102 (2013) 21902. doi:10.1063/1.4775677.
- [7] J. Tellinen, I. Suorsa, A. Jääskeläinen, I. Aaltio, K. Ullakko, Basic properties of magnetic shape memory actuators, in: 8th Int. Conf. ACTUATOR 2002, Bremen, 2002.
- [8] M. Chmielus, V.A. Chernenko, W.B. Knowlton, G. Kostorz, P. Müllner, Training, constraints, and high-cycle magneto-mechanical properties of Ni-Mn-Ga magnetic shape-memory alloys, Eur. Phys. J. Spec. Top. 158 (2008) 79–85. doi:10.1140/epjst/e2008-00657-3.
- [9] I. Aaltio, A. Soroka, Y. Ge, O. Söderberg, S.-P. Hannula, High-cycle fatigue of 10M Ni Mn–Ga magnetic shape memory alloy in reversed mechanical loading, Smart Mater. Struct. 19 (2010) 75014. doi:10.1088/0964-1726/19/7/075014.
- [10] K. Schlüter, B. Holz, A. Raatz, Principle Design of Actuators Driven by Magnetic Shape Memory Alloys, Adv. Eng. Mater. 14 (2012) 682–686. doi:10.1002/adem.201200078.
- [11] K. Ullakko, L. Wendell, A. Smith, P. Müllner, G. Hampikian, A magnetic shape memory micropump: contact-free, and compatible with PCR and human DNA profiling, Smart Mater. Struct. 21 (2012) 115020. doi:10.1088/0964-1726/21/11/115020.
- [12] I. Suorsa, J. Tellinen, K. Ullakko, E. Pagounis, Voltage generation induced by mechanical straining in magnetic shape memory materials, J. Appl. Phys. 95 (2004) 8054–8058. doi:10.1063/1.1711181.
- [13] D. Carpenter, M. Chmielus, A. Rothenühler, R. Schneider, P. Müllner, Application of Ferromagnetic Shape Memory Alloys in Power Generation Devices, in: G.B. Olson, D.S. Lieberman, A. Saxena (Eds.), Int. Conf. Martensitic Transform. 2008, John Wiley & Sons, Inc., Santa Fe, NM, 2008: pp. 365–369. http://iweb.tms.org/Purchase/ProductDetail.aspx?Product code=10-7452-365.
- [14] N. Lanska, O. Söderberg, A. Sozinov, Y. Ge, K. Ullakko, V.K. Lindroos, Composition and temperature dependence of the crystal structure of Ni–Mn–Ga alloys, J. Appl. Phys. 95 (2004) 8074. doi:10.1063/1.1748860.
- [15] O. Heczko, L. Straka, Temperature dependence and temperature limits of magnetic shape memory effect, J. Appl. Phys. 94 (2003) 7139–7143. doi:10.1063/1.1626800.
- [16] K. Ullakko, J.K. Huang, C. Kantner, R.C. O'Handley, V. V. Kokorin, Large magnetic-field-

- induced strains in Ni2MnGa single crystals, Appl. Phys. Lett. 69 (1996) 1966. doi:10.1063/1.117637.
- [17] A. Sozinov, A.A. Likhachev, K. Ullakko, Crystal structures and magnetic anisotropy properties of Ni-Mn-Ga martensitic phases with giant magnetic-field-induced strain, IEEE Trans. Magn. 38 (2002) 2814–2816. doi:10.1109/TMAG.2002.803567.
- [18] L. Straka, A. Soroka, H. Seiner, H. Hänninen, A. Sozinov, Temperature dependence of twinning stress of Type I and Type II twins in 10M modulated Ni-Mn-Ga martensite, Scr. Mater. 67 (2012) 25–28. doi:10.1016/j.scriptamat.2012.03.012.
- [19] U. Gaitzsch, M. Pötschke, S. Roth, B. Rellinghaus, L. Schultz, A 1% magnetostrain in polycrystalline 5M Ni–Mn–Ga, Acta Mater. 57 (2009) 365–370. doi:10.1016/j.actamat.2008.09.017.
- [20] M. Chmielus, X.X. Zhang, C. Witherspoon, D.C. Dunand, P. Müllner, Giant magnetic-field-induced strains in polycrystalline Ni-Mn-Ga foams, Nat. Mater. 8 (2009) 863–866. doi:10.1038/nmat2527.
- [21] M. Caputo, C.V. Solomon, P. Nguyen, A.E. Berkowitz, Electron Microscopy Investigation of Binder Saturation and Microstructural Defects in Functional Parts Made by Additive Manufacturing, in: Proc. Microsc. Microanal. 2016, Cambridge University Press, 2016: pp. 1770–1771. doi:10.1017/S1431927616009697.
- [22] A. Mostafaei, K.A. Kimes, E.L. Stevens, J. Toman, Y.L. Krimer, K. Ullakko, M. Chmielus, Microstructural evolution and magnetic properties of binder jet additive manufactured Ni-Mn-Ga magnetic shape memory alloy foam, Acta Mater. 131 (2017) 482–490. doi:10.1016/j.actamat.2017.04.010.
- [23] Y. Tian, D. Mcallister, H. Colijn, M. Mills, D. Farson, M. Nordin, S. Babu, Rationalization of Microstructure Heterogeneity in INCONEL 718 Builds Made by the Direct Laser Additive Manufacturing Process, Metall. Mater. Trans. A. 45A (2014) 4470. doi:10.1007/s11661-014-2370-6.
- [24] L. Costa, R. Vilar, T. Reti, A.M. Deus, Rapid tooling by laser powder deposition: Process simulation using finite element analysis, Acta Mater. 53 (2005) 3987–3999. doi:10.1016/j.actamat.2005.05.003.
- [25] B. Zheng, Y. Zhou, J.E. Smugeresky, J.M. Schoenung, E.J. Lavernia, Thermal Behavior and Microstructural Evolution during Laser Deposition with Laser-Engineered Net Shaping: Part I. Numerical Calculations, Metall. Mater. Trans. A. 39 (2008) 2228–2236. doi:10.1007/s11661-008-9557-7.
- [26] Y. Zhang, Z. Li, P. Nie, Y. Wu, Effect of cooling rate on the microstructure of laser-remelted INCONEL 718 coating, Metall. Mater. Trans. A Phys. Metall. Mater. Sci. 44A (2013) 5513–5521. doi:10.1007/s11661-013-1903-8.
- [27] P.A. Kobryn, E.H. Moore, S.L. Semiatin, The effect of laser power and traverse speed on microstructure, porosity, and build height in laser-deposited Ti-6Al-4V, Scr. Mater. 43 (2000) 299–305. doi:10.1016/S1359-6462(00)00408-5.
- [28] B.E. Carroll, T.A. Palmer, A.M. Beese, Anisotropic tensile behavior of Ti-6Al-4V components fabricated with directed energy deposition additive manufacturing, Acta Mater. 87 (2015) 309–320. doi:10.1016/j.actamat.2014.12.054.
- [29] C.M. Craciunescu, R.M. Miranda, R.J.C. Silva, E. Assuncao, F.M. Braz Fernandes, Laser beam interaction with Ni–Mn–Ga ferromagnetic shape memory alloys, Opt. Lasers Eng. 49 (2011) 1289–1293. doi:10.1016/j.optlaseng.2011.06.007.
- [30] C.A. Biffi, A. Tuissi, Fiber laser drilling of Ni46Mn27Ga27 ferromagnetic shape memory

- alloy, Opt. Laser Technol. 63 (2014) 1–7. doi:10.1016/j.optlastec.2014.03.010.
- [31] O. Heczko, P. Švec, D. Janičkovič, K. Ullakko, Magnetic properties of Ni-Mn-Ga ribbon prepared by rapid solidification, IEEE Trans. Magn. 38 (2002) 2841–2843. doi:10.1109/TMAG.2002.802471.
- [32] O. Söderberg, D. Brown, I. Aaltio, J. Oksanen, J. Syrén, H. Pulkkinen, S.-P. Hannula, Microstructure and properties of Ni–Mn–Ga alloys produced by rapid solidification and pulsed electric current sintering, J. Alloys Compd. 509 (2011) 5981–5987. doi:10.1016/j.jallcom.2011.02.166.
- [33] J. Wang, C. Jiang, R. Techapiesancharoenkij, D. Bono, S.M. Allen, R.C. O'Handley, Microstructure and magnetic properties of melt spinning Ni-Mn-Ga, Intermetallics. 32 (2013) 151–155. doi:10.1016/j.intermet.2012.08.021.
- [34] D.D. Gu, W. Meiners, K. Wissenbach, R. Poprawe, Laser additive manufacturing of metallic components: materials, processes and mechanisms, Int. Mater. Rev. 57 (2012) 133–164. doi:10.1179/1743280411Y.0000000014.
- [35] M. Richard, J. Feuchtwanger, D. Schlagel, T. Lograsso, S.M. Allen, R.C. O'Handley, Crystal structure and transformation behavior of Ni–Mn–Ga martensites, Scr. Mater. 54 (2006) 1797–1801. doi:http://dx.doi.org/10.1016/j.scriptamat.2006.01.033.
- [36] V.C. Solomon, D.J. Smith, Y. Tang, A.E. Berkowitz, Microstructural characterization of Ni-Mn-Ga ferromagnetic shape memory alloy powders, J. Appl. Phys. 95 (2004) 6954– 6956. doi:10.1063/1.1687204.
- [37] M. Pötschke, U. Gaitzsch, S. Roth, B. Rellinghaus, L. Schultz, Preparation of melt textured Ni-Mn-Ga, J. Magn. Magn. Mater. 316 (2007) 383–385. doi:10.1016/j.jmmm.2007.03.032.
- [38] K. Rolfs, M. Chmielus, J.M. Guldbakke, R.C. Wimpory, A. Raatz, W. Petry, P. Mullner, R. Schneider, Key properties of Ni-Mn-Ga based single crystals grown with the SLARE technique, Adv. Eng. Mater. 14 (2012) 614–635. doi:10.1002/adem.201200065.
- [39] P. Rangaswamy, M.L. Griffith, M.B. Prime, T.M. Holden, R.B. Rogge, J.M. Edwards, R.J. Sebring, Residual stresses in LENS® components using neutron diffraction and contour method, Mater. Sci. Eng. A. 399 (2005) 72–83. doi:10.1016/j.msea.2005.02.019.
- [40] V.A. Chernenko, M. Kohl, V.A. L'Vov, V.M. Kniazkyi, M. Ohtsuka, O. Kraft, Martensitic Transformation and Microstructure of Sputter-Deposited Ni–Mn–Ga Films, Mater. Trans. 47 (2006) 619–624. doi:10.2320/matertrans.47.619.
- [41] S. Doyle, V.A. Chernenko, S. Besseghini, A. Gambardella, M. Kohl, P. Müllner, M. Ohtsuka, Residual stress in Ni-Mn-Ga thin films deposited on different substrates, Eur. Phys. J. Spec. Top. 158 (2008) 99–105. doi:10.1140/epjst/e2008-00660-8.
- [42] O. Heczko, M. Thomas, J. Buschbeck, L. Schultz, S. Fähler, Epitaxial Ni-Mn-Ga films deposited on Sr Ti O 3 and evidence of magnetically induced reorientation of martensitic variants at room temperature, Appl. Phys. Lett. 92 (2008) 72502. doi:10.1063/1.2883961.
- [43] P. Müllner, G. Kostorz, Microstructure of Magnetic Shape-Memory Alloys: Between Magnetoelasticity and Magnetoplasticity, Mater. Sci. Forum. 583 (2008) 43–65. doi:10.4028/www.scientific.net/MSF.583.43.
- [44] P. Lázpita, J.M. Barandiarán, J. Gutiérrez, J. Feuchtwanger, V.A. Chernenko, M.L. Richard, Magnetic moment and chemical order in off-stoichiometric Ni-Mn-Ga ferromagnetic shape memory alloys, New J. Phys. 13 (2011) 33039. doi:10.1088/1367-2630/13/3/033039.
- [45] D. Kellis, A. Smith, K. Ullakko, P. Müllner, Oriented single crystals of Ni–Mn–Ga with very low switching field, J. Cryst. Growth. 359 (2012) 64–68. doi:10.1016/j.jcrysgro.2012.08.014.

- [46] J.D. Livingston, A review of coercivity mechanisms (invited), J. Appl. Phys. 52 (1981) 2544–2548. doi:10.1063/1.328996.
- [47] C. Jiang, Y. Muhammad, L. Deng, W. Wu, H. Xu, Composition dependence on the martensitic structures of the Mn-rich NiMnGa alloys, Acta Mater. 52 (2004) 2779–2785. doi:10.1016/j.actamat.2004.02.024.
- [48] M.L. Richard, Systematic analysis of the crystal structure, chemical ordering, and microstructure of Ni–Mn–Ga ferromagnetic shape memory alloys, Massachusetts Institute of Technology, 2005.
- [49] U. Gaitzsch, R. Chulist, L. Weisheit, A. Böhm, W. Skrotzki, C.-G. Oertel, H.-G. Brokmeier, T. Lippmann, I. Navarro, M. Pötschke, J. Romberg, C. Hürrich, S. Roth, L. Schultz, Processing Routes Toward Textured Polycrystals in Ferromagnetic Shape Memory Alloys, Adv. Eng. Mater. 14 (2012) 636–652. doi:10.1002/adem.201200084.
- [50] U. Gaitzsch, S. Roth, B. Rellinghaus, L. Schultz, Adjusting the crystal structure of NiMnGa shape memory ferromagnets, J. Magn. Magn. Mater. 305 (2006) 275–277. doi:10.1016/j.jmmm.2006.01.017.